

An estimate of anthropogenic CO₂ inventory from decadal changes in oceanic carbon content

Toste Tanhua, Arne Körtzinger, Karsten Friis, Darryn W. Waugh, and Douglas W. R. Wallace

PNAS published online Feb 20, 2007;
doi:10.1073/pnas.0606574104

This information is current as of February 2007.

Supplementary Material	Supplementary material can be found at: www.pnas.org/cgi/content/full/0606574104/DC1 This article has been cited by other articles: www.pnas.org#otherarticles
E-mail Alerts	Receive free email alerts when new articles cite this article - sign up in the box at the top right corner of the article or click here .
Rights & Permissions	To reproduce this article in part (figures, tables) or in entirety, see: www.pnas.org/misc/rightperm.shtml
Reprints	To order reprints, see: www.pnas.org/misc/reprints.shtml

Notes:

An estimate of anthropogenic CO₂ inventory from decadal changes in oceanic carbon content

Toste Tanhua[†], Arne Körtzinger[†], Karsten Friis[†], Darryn W. Waugh[‡], and Douglas W. R. Wallace^{†§}

[†]Leibniz-Institut für Meereswissenschaften, Marine Biogeochemie, Düsternbrooker Weg 20, 24105 Kiel, Germany; and [‡]Department of Earth and Planetary Sciences, Johns Hopkins University, Baltimore, MD 21218

Edited by David M. Karl, University of Hawaii, Honolulu, HI, and approved December 17, 2006 (received for review August 8, 2006)

Increased knowledge of the present global carbon cycle is important for our ability to understand and to predict the future carbon cycle and global climate. Approximately half of the anthropogenic carbon released to the atmosphere from fossil fuel burning is stored in the ocean, although distribution and regional fluxes of the ocean sink are debated. Estimates of anthropogenic carbon (C_{ant}) in the oceans remain prone to error arising from (i) a need to estimate preindustrial reference concentrations of carbon for different oceanic regions, and (ii) differing behavior of transient ocean tracers used to infer C_{ant} . We introduce an empirical approach to estimate C_{ant} that circumvents both problems by using measurement of the decadal change of ocean carbon concentrations and the exponential nature of the atmospheric C_{ant} increase. In contrast to prior approaches, the results are independent of tracer data but are shown to be qualitatively and quantitatively consistent with tracer-derived estimates. The approach reveals more C_{ant} in the deep ocean than prior studies; with possible implications for future carbon uptake and deep ocean carbonate dissolution. Our results suggest that this approach applied on the unprecedented global data archive provides a means of estimating the C_{ant} for large parts of the world's ocean.

anthropogenic carbon | marine chemistry | North Atlantic

The control of atmospheric CO₂ is the most technologically and economically challenging environmental mitigation task ever envisioned. Assessment of the effectiveness of policies and technologies requires ability to track anthropogenic CO₂ through rapidly exchanging atmospheric, oceanic, and terrestrial carbon reservoirs. Carbon in the “well mixed” atmosphere, with CO₂ as the major carbon species, is already monitored to high accuracy (e.g., ref. 1), whereas the complexity of the terrestrial carbon reservoir necessitates indirect approaches (e.g., ref. 2) or budgets involving scaling from local to global scales. The ocean, with intermediate spatial variability and carbon in a limited number of forms, is amenable to global measurement. Observational methods used to estimate anthropogenic carbon (C_{ant}) within the ocean fall into two categories: back calculations (3–5) based on measurements of inorganic carbon, and tracer approaches (6–9) based on measurement of anthropogenic tracers such as the chlorofluorocarbons (CFCs). The back calculations require estimates of “preindustrial reference concentrations” for carbon in different parts of the ocean against which modern measured carbon concentrations are compared. One particularly important method, the ΔC^* method (5), is the basis for a ground-breaking estimate of the global distribution of C_{ant} (10). Although this method utilizes carbon data, it shares similarities with proxy-based estimates based on CFCs (11, 12). The effects of required assumptions and error sources for the ΔC^* method have been critically examined (13) by using an ocean carbon model, identifying a significant positive bias in young waters and a small negative bias in older waters. Estimates of C_{ant} diverge particularly in the Southern Ocean, where both models and back-calculation methods vary widely, even when applied to the same data set (14).

Tracer approaches benefit from preindustrial tracer levels having been either zero or capable of estimation. However, these approaches have the disadvantage that tracers do not perfectly mimic C_{ant} in terms of atmospheric history and air–sea exchange characteristics. Because of the relatively recent introduction of most such tracers (i.e., CFCs; bomb ¹⁴C), there may be large volumes of the deep ocean with significant C_{ant} levels but zero levels of tracers (15, 16). Where tracers are present, transfer functions are required to derive C_{ant} estimates from the tracer data, and these depend critically on the representation of water mass age distributions within the ocean interior (8). Significant differences between various methods of estimating C_{ant} are evident. For instance, a tracer based estimate of the global C_{ant} inventory found large differences compared with ΔC^* based inventories (up to $\approx 50 \text{ mol m}^{-2}$), particularly for the Southern Ocean (17).

Results and Discussion

Anthropogenic Carbon Calculations. We will here estimate C_{ant} empirically from measurement of the temporal increase of carbon, ΔC_{ant} , using repeated ocean carbon surveys (18–20). For this purpose, we use inorganic carbon measurements made in the midlatitude North Atlantic during the Transient Tracers in the Ocean–North Atlantic Study (TTO-NAS) survey in 1981 and during the M60/5 cruise in 2004 (16), which reoccupied the exact locations of 27 of the earlier TTO-NAS stations (Fig. 1 *Upper*). The North Atlantic is a region with relatively well ventilated deep waters, and with deep penetration of C_{ant} , and is thus suitable for this study. The consistency between the TTO-NAS carbon data and modern data has been evaluated (21), and these data likely offer the best-available combination of historical data quality and time-difference between repeat surveys that is available for illustration of the method. Natural variations in carbon associated with the ocean's solubility and biological pumps are compensated for by using multiple linear regressions (MLRs); an approach introduced by Wallace (22) and extended by Friis *et al.* (11), here referred to as extended MLR (eMLR). In using eMLR for determining ΔC_{ant} , MLRs are established that relate measured dissolved inorganic carbon (DIC) concentrations with a set of hydrochemical parameters (p) measured on the same samples:

$$DIC = a_0 + a_1 \times p_1 + \dots + a_n \times p_n + R, \quad [1]$$

Author contributions: D.W.R.W. and K.F. designed research; T.T. and D.W.R.W. performed research; T.T., A.K., K.F., D.W.W., and D.W.R.W. analyzed data; and T.T., A.K., and D.W.R.W. wrote the paper.

The authors declare no conflict of interest.

This article is a PNAS direct submission.

Freely available online through the PNAS open access option.

Abbreviations: C_{ant} , anthropogenic carbon; MLR, multiple linear regression; eMLR; extended MLR; TTD, transit time distribution; CFC, chlorofluorocarbon; DIC, dissolved inorganic carbon; TTO-NAS, Transient Tracers in the Ocean–North Atlantic Study.

[§]To whom correspondence should be addressed. E-mail: dwallace@ifm-geomar.de.

This article contains supporting information online at www.pnas.org/cgi/content/full/0606574104/DC1.

© 2007 by The National Academy of Sciences of the USA

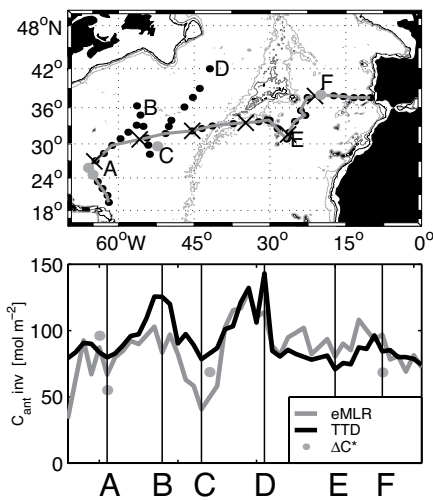


Fig. 1. Depth-integrated, water-column inventories of C_{ant} across the mid-latitude North Atlantic. (Upper) Track of RV Meteor's cruise M60/5 in 2004 (black dots). The letters refers to locations marked by lines in Lower, and the gray line is the location of the section, with a cross every 1,000 km. Light gray dots mark the location of the four cross-over stations between M60/5 and WOCE-lines used to calculate the global C_{ant} inventory (10). (Lower) Column inventory of C_{ant} (mol m^{-2}) along the cruise track calculated by the eMLR (gray line) and the TTD (black line) approaches. Marked as light gray dots are column inventories calculated from the ΔC^* method, downloaded from, http://cdiac.esd.ornl.gov/oceans/glodap/Glodap_home.htm and scaled to 2004 as a reference year (negative values not set to zero).

where R is the residual. Separate regression coefficients (a_0 to a_n) are established for the two time-separated surveys. Subtraction of the respective partial regression coefficients of the two models gives a new equation that relates only the temporal difference in DIC to the hydrochemical parameters. We interpret the so-calculated difference in DIC between the two surveys, $\Delta C_{\text{ant}}^{\text{eMLR}}$, as the change of inorganic carbon associated with the increase of anthropogenic CO_2 over the time period between the two surveys (i.e., ΔC_{ant}), (23, 24). To validate the eMLR method of calculating ΔC_{ant} , we compare the eMLR-derived differences to those derived from direct comparison of DIC values corrected for changes in remineralization of organic matter and calcium carbonate dissolution measured at exactly the same position (16). The values are compared on density rather than depth for the depth interval 200–2,000 m, values close to the surface and deep samples are compared by depth. The comparison of the two ways of calculating ΔC_{ant} (in Fig. 2) reveals a mean offset of $0.3 \mu\text{mol kg}^{-1}$ for the whole data set, suggesting that the two methods produce quantitatively similar results over the study area [see also supporting information (SI) Fig. 7].

We now explore the possibilities to extend the calculated ΔC_{ant} to cover the whole industrial uptake of carbon in the water column by applying the “transient steady state” concept originally proposed by Gammon *et al.* (25). The concept states that, after a period significantly longer than the exponential growth time scale of the tracer, the vertical tracer profiles reach transient steady state and have a constant “shape.” The tracer concentrations at all depths then increase at a rate that is proportional to the surface layer increase. In the case of steady transport the concentration of a tracer at location r is

$$c(r, t) = \int_0^{\infty} c_0(t - t')G(r, t) dt', \quad [2]$$

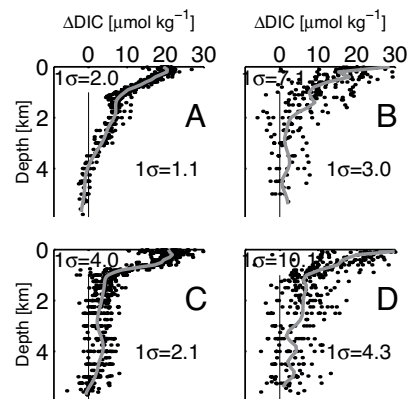


Fig. 2. ΔDIC in the North Atlantic between 1981 and 2001, from the eastern (A and B) and western (C and D) basins, with the same data used for both. A and C are calculated from the eMLR method, whereas B and D are calculated from the direct comparison method. One standard deviation of the estimates in surface and deep waters, respectively, are noted in the plot.

where $c_0(t)$ is the surface time history of the tracer and $G(r, t)$ is the transit time distribution (TTD) (8, 9). If the tracer concentration is exponentially changing, i.e., $c_0(t) = Ae^{\lambda t}$ then

$$c(r, t) = c_0(t) \int_0^{\infty} e^{-\lambda' G(r, t)} dt = c_0(t)F(r). \quad [3]$$

If we write the change in $c(r)$ over a given time period as $\Delta c(r) = c(r, t_2) - c(r, t_1)$ then we have

$$\Delta c(r) = \Delta c_0 F(r), \quad [4]$$

where $\Delta c_0 = c_0(t_2) - c_0(t_1)$. Combining Eqs. 3 and 4 gives

$$c(r, t) = \frac{c_0(t_2)\Delta c(r)}{\Delta c_0}. \quad [5]$$

Therefore, if $\Delta c(r)$ is measured, then $c(r, t)$ can be determined by using Eq. 5 with knowledge of $c_0(t_2)$ and $c_0(t_1)$. In other words, if C_{ant} can be treated as an exponentially increasing transient tracer and $\Delta C_{\text{ant}}^{\text{eMLR}}$ is measured from repeated sampling at a location r , then the total anthropogenic carbon, $C_{\text{ant}}^{\text{eMLR}}$, can be estimated from Eq. 5 for any given time with knowledge of the time-dependent surface C_{ant} history. The latter is readily calculated from the temporal increase of atmospheric CO_2 and the CO_2 solubility. This approach to calculate C_{ant} is based on carbon data and so does not require tracer–carbon transfer functions. Furthermore, it uses reference concentrations based on historical measurements, which precludes the need to estimate the (unknown) preindustrial carbon concentrations. The exponential growth of C_{ant} has also been used by, for instance, Bacastow and Keeling (26) to predict future CO_2 concentrations, and to scale CO_2 perturbations in models (e.g., refs. 27–29).

However, there remain a few assumptions and some error sources with this approach. First, temporal changes in seawater buffer capacity due to, for instance, the anthropogenic DIC perturbation in surface waters or temperature changes will affect $c_0(t)$. However, changes in the buffer capacity of seawater have a negligible effect on the $c_0(t_2)/\Delta c_0$ ratio, and certainly to a lesser extent than the analytical errors (SI Fig. 8). Therefore, it is justified to apply one constant (3.0) for the whole data set, independent of temperature and alkalinity at the time of equilibrium with the atmosphere.

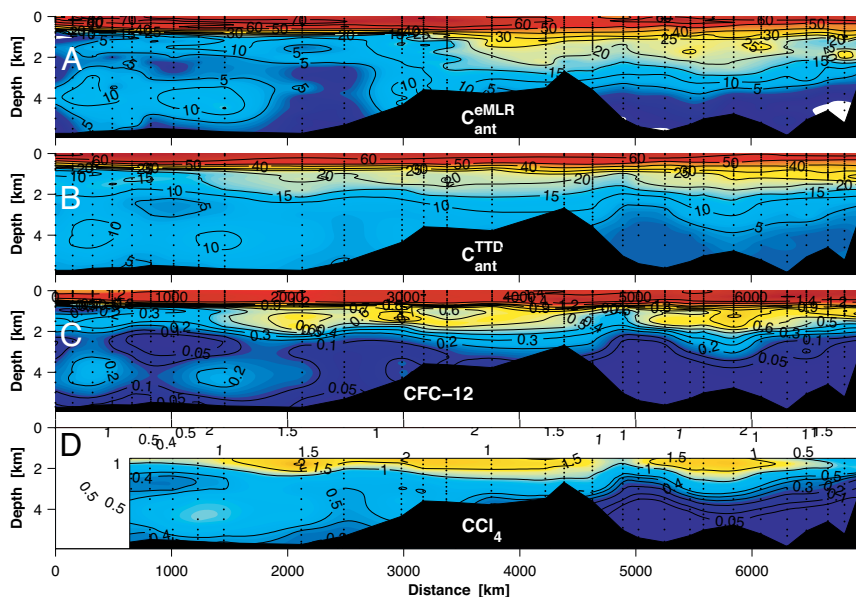


Fig. 3. Quasizonal sections across the midlatitude North Atlantic (see Fig. 1 for a map). (A and B) Concentrations of anthropogenic carbon in $\mu\text{mol kg}^{-1}$ as calculated with the TTD or the eMLR method. (C and D) Concentrations of the transient tracers CFC-12 and CCl_4 in pmol kg^{-1} . Only depths $>1,500$ m (the $\approx 5^\circ\text{C}$ isotherm) are shown for CCl_4 because it is rapidly hydrolyzed at higher temperatures (43).

Second, the transient steady state assumes perfectly exponential atmospheric increase of the tracer and is, strictly, achieved only some time after this tracer is introduced. The effect of any nonexponential increase of anthropogenic carbon in the atmosphere and the validity of scaling a measured ΔC_{ant} to the total C_{ant} can be tested by using specified TTDs (8, 30). For a given TTD, we first calculated a theoretical C_{ant} and ΔC_{ant} , from Eq. 2, assuming an inverse Gaussian TTD with the width (Δ) of the TTD being equal to the mean age (Γ) (30). We then used Eq. 5 to calculate C_{ant} from ΔC_{ant} . The agreement between the two ways of estimating C_{ant} is excellent, i.e., the difference between the two approaches is much smaller than errors in estimating ΔC_{ant} from measurements (SI Figs. 9 and 10). Furthermore, we have shown, using an eddy-permitting ocean general circulation model of the North Atlantic (FLAME $1/3^\circ$ model), that C_{ant} reaches “transient steady state” ≈ 50 years after the exponential increase is “switched-on” (16). The increase of surface ocean CO_2 has been exponential since about 1750, and concentrations 50 years later were still only $\approx 4 \mu\text{mol kg}^{-1}$, or $<7\%$, of present-day levels. Hence, the extrapolation errors associated with C_{ant} uptake during this early period when profiles were not yet in transient steady state, and the nonperfect exponential increase of C_{ant} , are small.

Thirdly, the time-evolution of surface C_{ant} depends on the assumption of constant CO_2 air–sea disequilibrium (13, 31). This is a problem common to all C_{ant} estimation approaches. The problem does not affect the estimate of $\Delta c(r)$, because this is measured, rather it affects the accuracy of the scaling factor $C_0(t_2)/\Delta C_0$. If the disequilibrium is changing or if it shows temporal variability, it will cause an error in the ratio $C_0(t_2)/\Delta C_0$, and hence in the $C_{\text{ant}}^{\text{eMLR}}$ calculation. The effects of changing air–sea disequilibrium on the scaling factor is best studied in an ocean model similar to the work by Matsumoto and Gruber (13). There are indications that the disequilibrium in the North Atlantic might have decreased rather than increased in recent decades (32, 33), which would lead to a small error in $C_{\text{ant}}^{\text{eMLR}}$. Temporal changes in the disequilibrium are, however, included in the measured decadal difference in DIC, so that the determination of C_{ant} by the eMLR method is relatively insensitive to

such temporal changes, provided that the ratio $C_0(t_2)/\Delta C_0$ is correctly determined.

North Atlantic Distribution. Here we apply the method proposed here to the TTD-NAS and M60/5 data sets. We have scaled the measured $C_{\text{ant}}^{\text{eMLR}}$ using Eq. 5 to calculate concentrations of anthropogenic CO_2 ($C_{\text{ant}}^{\text{eMLR}}$); these are plotted along a quasizonal section across the mid-latitude North Atlantic in Fig. 3A. The $C_{\text{ant}}^{\text{eMLR}}$ section can be directly compared with sections of the transient tracers CFC-12 and CCl_4 measured in 2004 as shown in Fig. 3C and D, noting that high tracer concentration indicate recently ventilated waters and therefore potentially higher levels of C_{ant} . There is excellent qualitative agreement between the tracer and $C_{\text{ant}}^{\text{eMLR}}$ distributions, especially in the deepest waters, where disagreement between various C_{ant} estimation methods tends to be greatest (17). Note, for instance, the correlation between elevated tracer and $C_{\text{ant}}^{\text{eMLR}}$ concentrations in the North Atlantic Deep Water (NADW) of the western basin at ≈ 4000 m depth. A series of maxima and minima are coincident even though the $C_{\text{ant}}^{\text{eMLR}}$ estimates are fully independent of the tracer data. In the eastern basin, $C_{\text{ant}}^{\text{eMLR}}$ concentrations around zero and $\text{CFC-12} < 0.01 \text{ pmol kg}^{-1}$ are found in the deepest waters. Even at these low levels, there is good correlation of the $C_{\text{ant}}^{\text{eMLR}}$ estimates with anthropogenic CCl_4 , the transient tracer with a history of input that extends back to 1910 (34) and which is therefore the best tracer for the presence of C_{ant} in slowly ventilated waters.

To make a more quantitative comparison between our C_{ant} estimates and the transient tracers, we compare $C_{\text{ant}}^{\text{eMLR}}$ with the C_{ant} concentrations calculated by using the transit time distribution TTD method ($C_{\text{ant}}^{\text{TTD}}$) (8, 9, 17). This method is completely independent of carbon measurements and the carbon-related parameters used in the back-calculation and eMLR methods. The $C_{\text{ant}}^{\text{TTD}}$ estimation is based exclusively on transient tracer data and assumptions concerning the distribution of transit times within interior ocean water masses. For these calculations, we used the CFC-12 data measured during M60/5 (16) and have assumed that water masses are formed with 90% saturation relative to atmospheric CFC levels (35). The effect of the saturation level assumption on the C_{ant} calculation is particularly

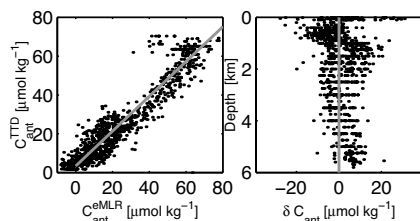


Fig. 4. Comparison between the $C_{\text{ant}}^{\text{TTD}}$ and $C_{\text{ant}}^{\text{eMLR}}$ estimates. (Left) The geometric mean linear regression is plotted in gray. (Right) The difference $C_{\text{ant}}^{\text{TTD}} - C_{\text{ant}}^{\text{eMLR}}$ (δC_{ant}) plotted vs. depth for the whole data set.

high in the recently ventilated waters due to the low CFC-12 and high C_{ant} atmospheric increase rate over the last ≈ 15 years, whereas the older water is relatively insensitive to small changes in saturation level. We have assumed that interior ocean TTDs can be approximated by inverse Gaussian functions with a fixed relation between the mean age and width of the TTD. We assume strong mixing, i.e., the TTD width equals the mean age of transit time distribution; this assumption has been shown to be consistent with transient tracer concentrations in the North Atlantic (9). The resulting quantitative agreement between the $C_{\text{ant}}^{\text{TTD}}$ and $C_{\text{ant}}^{\text{eMLR}}$ sections is, over all, remarkably good, as shown in Fig. 3 *A* and *B*. For instance, both methods indicate comparably high levels of C_{ant} ($> 10 \mu\text{mol kg}^{-1}$) in the NADW of the western basin. This finding is in contrast to sections of C_{ant} calculated with the ΔC^* method ($C_{\text{ant}}^{\Delta C^*}$) that do not show this high C_{ant} core in the NADW at this latitude (36). To evaluate the consistency between $C_{\text{ant}}^{\text{eMLR}}$ and the transient tracers, we compare the C_{ant} concentration calculated with the TTD and eMLR methods in Fig. 4. Fig. 4 *Left* shows the two estimates plotted vs. each other, the geometric mean linear correlation is $C_{\text{ant}}^{\text{TTD}} = (0.90 \pm 0.011) \times C_{\text{ant}}^{\text{eMLR}} + (3.41 \pm 0.24)$ and $r = 0.94$; and Fig. 4 *Right* shows the mean offset between the two methods to be $0.8 \mu\text{mol kg}^{-1}$, with a standard deviation of $7.9 \mu\text{mol kg}^{-1}$.

Despite the overall excellent agreement, there are also specific regions and water masses where systematic differences between the TTD- and eMLR-based C_{ant} estimates are observed. We first note the difference in the density range of the Labrador Sea Water (LSW) at $\approx 1,000$ - to $2,000$ -m depth. This difference may be attributable to the assumption by the TTD method of time-invariant air–sea disequilibrium. Increasing air–sea CO_2 disequilibrium with time has been anticipated (9, 13), even though decreasing disequilibrium has been shown for subpolar waters (33), so that this assumption would cause the TTD method to overestimate the C_{ant} concentration. Indeed, we find that, for this depth range, $C_{\text{ant}}^{\text{TTD}} - C_{\text{ant}}^{\text{eMLR}}$ is positive, suggesting that water masses formed by deep convection may be especially susceptible to a time-varying CO_2 air–sea disequilibrium. The eMLR method on the other hand is based on the measured, decadal, change of carbon concentration and should, in principle, incorporate such effects (see discussion above). In this case, the eMLR method may give the more accurate result.

The second area of obvious differences is for “old” waters (i.e., $\text{CFC-12} \approx 0.1 \text{ pmol kg}^{-1}$), where $C_{\text{ant}}^{\text{TTD}} - C_{\text{ant}}^{\text{eMLR}}$ averages $3.0 \pm 5.1 \mu\text{mol kg}^{-1}$. Determination of C_{ant} for old waters is difficult for any C_{ant} inference method; for the TTD method, this is primarily due to the different input functions of C_{ant} and the tracers available for oceanographic studies. For this work, we used CFC-12, which has an atmospheric history initiated in about 1950, which is in contrast to the length of anthropogenic CO_2 increase that started in the middle of the 18th century. For the older waters, the $C_{\text{ant}}^{\text{TTD}}$ concentration is thus dependent on CFC-12 values at the lower end of the measurable range. Due to difficulties in sampling and storing water samples, a sampling blank for CFC measurements cannot be ruled out, and the

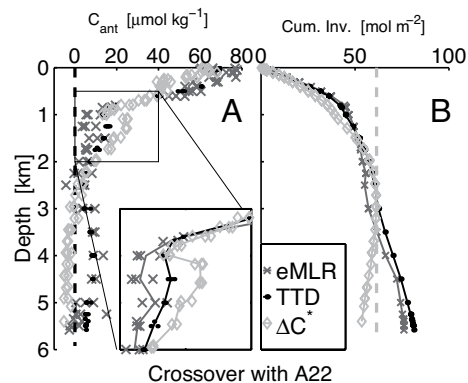


Fig. 5. C_{ant} calculated with the three different methods: eMLR (dark gray crosses), ΔC^* (light gray diamonds), and TTD (black dots) for the stations surrounding the crossover for cruise A22 at point “A” (Fig. 1). (A) C_{ant} vs. depth ($\mu\text{mol kg}^{-1}$) for the three methods with *Inset* showing a blown-up view of the layer between 500 and 2,000 m. (B) Cumulative C_{ant} inventory (mol m^{-2}) calculated for the three methods, the light gray dashed line marks the highest column inventory for the ΔC^* method, i.e., the value that is used in ref. 10 to calculate the global inventory, by setting negative values to zero.

difference in C_{ant} calculations for old waters may be associated with difficulties to correctly quantify the sampling blank. An underestimation of $\approx 0.005 \text{ pmol kg}^{-1}$ would lead to an overestimation of $C_{\text{ant}}^{\text{TTD}}$ by $\approx 3 \mu\text{mol kg}^{-1}$ for waters that are essentially free of CFC-12; but only $\approx 0.2 \mu\text{mol kg}^{-1}$ for waters with higher CFC-12 concentrations, due to the curvature in the relation between CFC-12 and C_{ant} (37).

Our best estimate of the overall accuracy of the eMLR based ΔC_{ant} is 1.3 and $0.6 \mu\text{mol kg}^{-1}$ (95% confidence interval) for the eastern and western basins, respectively, although this depends on basin and water mass (see *SI Text* and *SI Figs. 11–15*). The results shown in the *SI* should be used as guidance for determining the significance of the eMLR derived ΔC_{ant} estimate for specific regions or water masses. The uncertainty with extrapolating the ΔC_{ant} to the full range of C_{ant} is a factor of 3 larger, and the overall accuracy of the $C_{\text{ant}}^{\text{eMLR}}$ concentration is thus likely

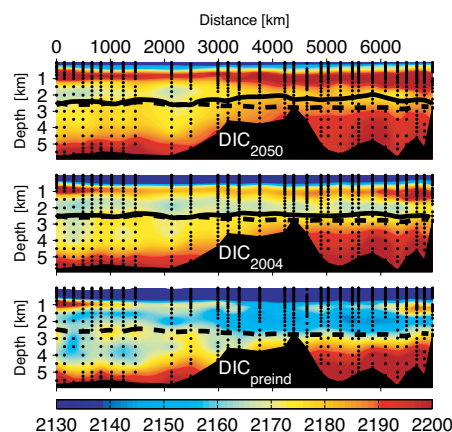


Fig. 6. DIC concentration ($\mu\text{mol kg}^{-1}$) and the aragonite saturation horizon calculated by using the CO2SYS program (44) for the section across the North Atlantic for preindustrial conditions (*Bottom*), the situation in 2004 (*Middle*), and the projected DIC concentration in 2050 assuming continued exponential atmospheric increase of C_{ant} (i.e., 460 ppm CO_2) (*Top*). The preindustrial saturation horizon is marked with a black dashed line, and the solid black lines are the aragonite saturation horizon in 2004 and 2050, respectively. All calculations assume no changes in circulation, biology, alkalinity, and temperature compared with 2004.

Table 1. The coefficients (a_0 to a_n) for the MLRs used to quantify decadal change in DIC together with the regression coefficient (R^2) and the number of samples (n) for the regression given in Eq. 1

Data set	a_0	A_T	AOU	θ	NO_3	SiO_2	n	R^2
TTO, EB	327 ± 69	0.760 ± 0.029	0.186 ± 0.072	-3.56 ± 0.37	4.86 ± 0.56	-0.686 ± 0.061	437	0.992
M60/5, EB	729 ± 105	0.594 ± 0.045	0.364 ± 0.106	-2.89 ± 0.56	3.33 ± 0.81	-0.629 ± 0.101	387	0.976
TTO, WB	595 ± 53	0.662 ± 0.022	0.570 ± 0.038	-6.30 ± 0.20	1.80 ± 0.30	-0.620 ± 0.045	980	0.989
M60/5, WB	$1,647 \pm 202$	0.232 ± 0.087	0.838 ± 0.059	-4.85 ± 0.44	-1.24 ± 0.50	-0.078 ± 0.125	652	0.978

not better than $\approx 5 \mu\text{mol kg}^{-1}$. The error is not necessarily associated with errors in the carbon measurements because these can be assessed (21). Rather, the accuracy and internal consistency of the other oceanographic parameters used for the multiple regressions may be even more important. The application of the eMLR method in deep waters is particularly sensitive to systematic measurement biases in nutrient data between surveys (low C_{ant} waters usually also have high nutrient values). Nutrient data are notoriously error-prone (38) in part because of technique variations between groups and a continued lack of generally accepted and widely used reference materials. Effort has to be made to check the consistency of these supporting data; preferably by better standardization and by the use of certified reference materials.

We also compare the column inventories of C_{ant} calculated with the two methods, as well as with the application of the ΔC^* method ($C_{\text{ant}}^{\Delta C^*}$) that were used to calculate the global C_{ant} inventory (10) at four cross-over stations between the M60/5 and WOCE-lines. The latter have been scaled to 2004 (assuming transient steady state) as a reference year to make them directly comparable to our M60/5 data. As shown in Fig. 1 *Lower*, the column inventory of C_{ant} from Sabine *et al.* (10) is not significantly different from those calculated with the TTD and the eMLR methods. However, there are significant differences in the distribution of the C_{ant} with depth as shown in Fig. 5 (see also SI Figs. 16–18). The $C_{\text{ant}}^{\Delta C^*}$ profiles at the cross-over station have zero and even negative values below $\approx 2,500$ m, which is clearly contradicted by the tracer data. Hence, this application of ΔC^* (10) is likely in error for the North Atlantic deep waters. For the $C_{\text{ant}}^{\Delta C^*}$ inventory calculations in ref. 10, negative values of C_{ant} were set to zero, resulting in the column inventory marked as a dashed line in Fig. 5B. On the other hand, the ΔC^* method tends to overestimate the C_{ant} concentration in the intermediate waters of the western basin due to the combined effects of the assumptions of constant air–sea disequilibrium (13) and unrealistically low mixing (12, 16). For the cross-over stations this is particularly noticeable in the 1,000–2,000 m depth interval, where also a $\approx 10 \mu\text{mol kg}^{-1}$ discontinuity in $C_{\text{ant}}^{\Delta C^*}$ is found (17); this is associated with a change in methodology to calculate $C_{\text{ant}}^{\Delta C^*}$ at the corresponding density level.

Implications. We have shown that the column inventory is similar between the methods of calculating C_{ant} . However, this similarity is due to compensating errors, and the difference in allocation of C_{ant} with depth has potential implications for future projections of oceanic C_{ant} uptake. The “rapid filling” of the upper ocean implied by the ΔC^* results means a more rapid decrease in upper ocean buffer capacity and hence more rapid decrease in future ocean uptake. On the other hand, the eMLR and TTD results suggest a broader distribution of C_{ant} through the North Atlantic water column, implying that North Atlantic uptake might be less limited by changes in the carbonate system chemistry of the upper water column. Our results also imply that more anthropogenic carbon is entering deeper parts of the ocean close to the calcite and aragonite saturation horizons: This finding suggests more potential for dissolving carbonate depos-

its, that in turn will restore oceanic C_{ant} uptake capacity on millennial time scales but may have negative impact on calcifying deep water corals (39, 40). Over the mid-Atlantic Ridge and in the eastern basin, we find relatively shallow penetration of C_{ant} , which will thus mainly affect the aragonite saturation horizon (Fig. 6). We calculate that the saturation horizon for aragonite has shoaled ≈ 400 m since preindustrial times (40, 41), which we project will increase to ≈ 700 m by the year 2050, assuming continued exponential increase of C_{ant} . For the western basin, however, our calculations indicate only modest mid-depth C_{ant} uptake and thus a small effect on the aragonite saturation horizon, but ≈ 200 m shoaling of the calcite saturation horizon (that is located deeper than the aragonite saturation horizon) due to the deep penetration of C_{ant} . The deep penetration of C_{ant} in our calculations is probably of most importance for areas with recently ventilated deep waters such as the North Atlantic. The eMLR method has the potential to solve the question of the Southern Ocean C_{ant} uptake.

Our results suggest that by accurately measuring the ΔC_{ant} over decadal timescales, the global C_{ant} inventory and distribution can be determined, potentially with reduced uncertainty and with fewer problematic assumptions (11). A prerequisite is global coverage of high-quality repeat hydrochemical data with attention not only to the carbonate system but also to nutrient and oxygen measurements, preferably with certified reference materials to assure consistency.

Materials and Methods

eMLR. The choice of parameters for the eMLR analysis is highly dependent on the quality of the measurements and on ocean basin, and has to be determined from case to case. For this study we used potential temperature, alkalinity, silicate, nitrate, and apparent oxygen utilization to adequately characterize the water properties to calculate the DIC, and we made separate correlations for the eastern and western basin due to the different oceanographic conditions (see Table 1 for the coefficients a_0 to a_n used in Eq. 1).

Chemical Measurements. The CFC measurements performed during M60/5 were made on an analytical system similar to that described by Bullister and Weiss (42) and are reported on the SIO98 scale. The analytical precision was determined to be 0.7 and 0.6% for CFC-12 and CFC-11, respectively, as calculated from duplicate samples. We have subtracted a CFC-12 sampling blank of $0.007 \text{ pmol kg}^{-1}$, determined as the median value of 18 deep water samples in the eastern basin.

Details of the DIC and alkalinity measurements during M60/5 and TTO-NAS are given in refs. 16 and 21. Oxygen measurements were performed with Winkler titration, whereas the nutrients were measured on an autoanalyzer. We checked the consistency of the nutrients and oxygen measurements with crossover stations of three US-CLIVAR cruises occupied during 2003 (A16, A20, and A22). We found the M60/5 silicate data to be up to $2.0 \mu\text{mol kg}^{-1}$ lower, and nitrate up to $0.5 \mu\text{mol kg}^{-1}$ lower than the CLIVAR crossovers in the high concentration range. We corrected our data accordingly, which also made the

M60/5 data consistent with the TTO-NAS data in the deep waters of the eastern basin.

This analysis is only possible because of the painstaking work of the TTO-NAS planners, shipboard teams, and measurement groups of the

1980s who bequeathed an astonishingly high-quality data set to future generations. Acknowledgments are also due to the scientists, technicians, crew, officers, and Captain Jakobi of Meteor Cruise 60/5. Funding was provided from Deutsche Forschungsgemeinschaft (DFG) through SFB460 and grants for the M60/5 field program.

1. Keeling CD, Whorf TP (2005) in *Trends: A Compendium on Global Data, Carbon Dioxide Analysis Center* (Oak Ridge National Laboratory, US Dept of Energy, Oak Ridge, TN).
2. Keeling RF, Piper SC, Heimann M (1996) *Nature* 381:218–221.
3. Brewer PG (1978) *Geophys Res Lett* 5:991–1000.
4. Chen C-T, Millero F (1979) *Nature* 277:205–206.
5. Gruber N, Sarmiento JL, Stocker TF (1996) *Global Biogeochem Cycles* 10:809–837.
6. McNeil BI, Matear RJ, Key RM, Bullister JL, Sarmiento JL (2003) *Science* 299:235–239.
7. Thomas H, Ittekkot V (2001) *J Marine Syst* 27:325–336.
8. Hall TM, Haine TN, Waugh DW (2002) *Global Biogeochem Cycles* 16:1131.
9. Waugh DW, Hall TM, Haine TWN (2004) *Deep-Sea Res I* 51:1471–1491.
10. Sabine CL, Feely RA, Gruber N, Key RM, Lee K, Bullister JL, Wanninkhof R, Wong CS, Wallace DWR, Tilbrook B, et al. (2004) *Science* 305:367–371.
11. Friis K, Körtzinger A, Pätsch J, Wallace DWR (2005) *Deep-Sea Res I* 52:681–698.
12. Keeling RF (2005) *Science* 308:1743c.
13. Matsumoto K, Gruber N (2005) *Global Biogeochem Cycles* 19:GB3014.
14. Lo Monaco C, Goyet C, Metzl N, Poisson A, Tourtier F (2005) *J Geophys Res* 110:C09S02.
15. Wallace DWR (2001) in *Ocean Circulation and Climate*, ed Church JS, Gould J (Academic, New York), pp 489–521.
16. Tanhua T, Biastoch A, Körtzinger A, Lüger H, Böning C, Wallace DWR (2006) *Global Biogeochem Cycles* 20:GB4017.
17. Waugh DW, Hall TM, McNeil BI, Key R, Matear RJ (2006) *Tellus B* 58:376–389.
18. Peng, T.-H., Wanninkhof R, Bullister JL, Feely RA, Takahashi T (1998) *Nature* 396:560–563.
19. Matear RJ, McNeil BI (2003) *Global Biogeochem Cycles* 17:24.
20. McNeil BI, Tilbrook B, Matear R (2001) *J Geophys Res* 106:31431–31445.
21. Tanhua T, Wallace DWR (2005) *Geophys Res Lett* 32:L14618.
22. Wallace DWR (1995) *Monitoring Global Ocean Carbon Inventories* (Texas A&M University, Collage Station, TX).
23. Friis K (2006) *Tellus B* 582–15.
24. Sabine CL, Gruber N (2005) *Science* 308:1743d.
25. Gammon RH, Cline J, Wisegarver DP (1982) *J Geophys Res* 87:9441–9454.
26. Bacastow RB, Keeling CD (1979) in *Carbon Dioxide Effects Research and Assessment Program/Workshop on the Global Effects of Carbon Dioxide from Fossil Fuels*, ed Elliott WP (U.S. Dept of Energy, Washington, DC), pp 72–90.
27. Holfort J, Johnson KM, Putzka A, Schneider B, Siedler G, Wallace DWR (1988) *Global Biogeochem Cycles* 12:479–499.
28. Mikaloff Fletcher SE, Gruber N, Jacobson AR, Doney SC, Dutkiewicz S, Gerber M, Follows M, Joos F, Lindsay K, Menemenlis D, et al. (2006) *Global Biogeochem Cycles* 20:GB2002.
29. Gloor M, Gruber N, Sarmiento J, Sabine CL, Feely RA, Rodenbeck C (2003) *Geophys Res Lett* 30:10.1029/2002GL015594.
30. Waugh DW, Hall TM, Haine TWN (2003) *J Geophys Res* 108.
31. Hall TM, Waugh DW, Haine TWN, Robbins PE, Khatiwala S (2004) *Global Biogeochem Cycles* 18:GB1031.
32. Lefèvre N, Watson A, Olsen A, Rios AF, Pérez FF, Johannessen T (2004) *Geophys Res Lett* 31:L07306.
33. Omar AM, Olsen A (2006) *Geophys Res Lett* 33:L04602.
34. Krysell M, Wallace DWR (1988) *Science* 242:746–749.
35. Mecking S, Warner MJ, Bullister JL (2006) *Deep-Sea Res I* 53:169–187.
36. Lee K, Choi S-D, Park G-H, Wanninkhof R, Peng TH, Key RM, Sabine CL, Feely RA, Bullister JL, Millero FJ, Kozyr A (2003) *Global Biogeochem Cycles* 17:1116.
37. Körtzinger A, Rhein M, Mintrop L (1999) *Geophys Res Lett* 26:2065–2068.
38. Gruber N, Keller K, Key RM (2000) *Science* 290:455–456.
39. Guinotte JM, Orr J, Cairns S, Freiwald A, Morgan L, George R (2006) *Frontiers Ecol Environ* 4:141–146.
40. Orr JC, Fabry VJ, Aumont O, Bopp L, Doney SC, Feely RA, Gnanadesikan A, Gruber N, Ishida A, Joos F, et al. (2005) *Nature* 437:681–686.
41. Feely RA, Sabine CL, Lee K, Berelson W, Kleypas J, Fabry VJ, Millero FJ (2004) *Science* 305:362–366.
42. Bullister JL, Weiss RF (1988) *Deep-Sea Res* 35:839–853.
43. Jeffers PM, Brenner C, Wolfe NL (1996) *Environ Toxicol Chem* 15:1064–1065.
44. Lewis E, Wallace DWR (1998) *Program Developed for CO₂ System Calculations (ORNL/CDIAC-105)* (Oak Ridge National Laboratory, US Dept of Energy, Oak Ridge, TN), <http://cdiac.ornl.gov/oceans/co2rprt.html>.